Journal of Catalysis 277 (2011) 104–116

Contents lists available at ScienceDirect

Journal of Catalysis

journal homepage: www.elsevier.com/locate/jcat

Dehydrogenation of propane over Zn—MOR. Static and dynamic reaction energy diagram

L. Benco [a,b,*], T. Bucko [c], J. Hafner [a]

[a] Computational Materials Physics, Faculty of Physics, Vienna University, Sensengasse 8, A-1090 Vienna, Austria
[b] Institute of Inorganic Chemistry, Slovak Academy of Sciences, Dubravska cesta 9, SK-84536 Bratislava, Slovakia
[c] Department of Physical and Theoretical Chemistry, Faculty of Natural Sciences, Comenius University, Mlynska Dolina, SK-84215 Bratislava, Slovakia

ARTICLE INFO

Article history:
Received 29 July 2010
Revised 27 September 2010
Accepted 23 October 2010

Keywords:
Propane dehydrogenation
Zn-exchanged zeolite
Periodical DFT calculation
Cluster model
Harmonic transition state theory
Thermodynamic integration

ABSTRACT

The dehydrogenation of propane over Zn^{2+}-exchanged mordenite has been studied theoretically using ab initio density-functional calculations at different levels of theory. We compare (i) total-energy calculations based on semilocal exchange-correlation functionals with those adding semi-empirical corrections for dispersion forces, (ii) calculations based on a large periodic model of the zeolite with calculations based on small and large finite cluster models, and (iii) calculations of the free energies of activation and of the reaction rates based on harmonic transition state theory (hTST) with those based on thermodynamic integration over free-energy gradients determined by constrained ab initio molecular dynamics. Dehydrogenation proceeds in four steps: (i) adsorption of propane on the Zn^{2+} cation, (ii) dissociation of a hydrogen atom leading to the formation of a Zn-propyl complex and a Brønsted acid site, (iii) reaction of the acid proton and a β–H atom of propyl, resulting in the elimination of a hydrogen molecule, and (iv) desorption of propene from the Zn^{2+} cation.

The periodic calculations demonstrate that the dispersion corrections increase the adsorption/desorption energies from 70 to 107 kJ/mol for propane and from 177 to 233 kJ/mol for propene and decrease the activation energy for H-dissociation from 73 to 61 kJ/mol, while the activation energy for the heterolytic dehydrogenation is almost unaffected with 132 kJ/mol. Hence, dispersion corrections are of foremost importance for lowering the activation energy for H-dissociation below the desorption energy of propane. While according to the periodic calculations the highest activation energies are predicted for the heterolytic dehydrogenation and the desorption of propene, cluster calculations predict a higher activation energy for H-dissociation than for H_2 elimination. Both hTST and thermodynamic integrations show that both activation processes lead to a loss of entropy because the transition state configurations admit for a lower degree of disorder than the initial and intermediate states. hTST consistently underestimates the loss of entropy, the anharmonic corrections are most important for the H-dissociation step.

1. Introduction

The ability of Zn-exchanged zeolites to dehydrogenate is important for the catalytic conversion of alkanes [1,2]. Many studies tried to identify the nature of the active Zn-species and showed that besides the bare divalent Zn^{2+} cation [3–10] charged $[Zn—O—Zn]^{2+}$ particles exist under oxidizing conditions [4,11]. The comparison of the properties of these two species led to the conclusion that the bare Zn^{2+} cation is the most probable active site for the dehydrogenation of light alkanes [2].

The mechanism of the dehydrogenation of light alkanes over Zn-exchanged zeolites was studied both experimentally [7,12,13] and theoretically [14–16]. Molecular adsorption of an alkane on the active site results already at moderate temperatures in a heterolytic dissociation into a propyl anion bound to the cation and a hydrogen atom forming a Brønsted acid site by binding to an activated oxygen atom next to an Al/Si substitution site [17–20]. At increased temperatures, the acid proton reacts with a β-H atom of the propyl, leading to the formation of a hydrogen molecule and a propene molecule adsorbed at the cation. All steps of this reaction have been investigated using quantum-chemical methods. The first theoretical study of the dehydrogenation of an alkane over a Zn^{2+} cation by Frash and van Santen [14] used an extremely small cluster consisting of the four-membered ring with two Si and two Al atoms and the Zn^{2+} cation connected to four O atoms of the ring. Along the reaction path, dehydrogenation is the rate-limiting step with an activation energy of ~224 kJ/mol for ethane. The following studies by van Santen and co-workers [15,16] used a cluster consisting of two five-membered rings and a $[Zn—O—Zn]^{2+}$ complex

* Corresponding author at: Computational Materials Physics, Faculty of Physics, Vienna University, Sensengasse 8, A-1090 Vienna, Austria. Fax: +43 1 4277 9514.
E-mail addresses: Lubomir.Benco@univie.ac.at (L. Benco), Tomas.Bucko@univie.ac.at (T. Bucko), Juergen.Hafner@univie.ac.at (J. Hafner).

0021-9517/$ - see front matter © 2010 Elsevier Inc. All rights reserved.
doi:10.1016/j.jcat.2010.10.018

as the active site [15,16], leading a lower activation energy of ~200 kJ/mol. Recently, a comprehensive study by Pidko and van Santen [21] compared the dehydrogenation of ethane over different Zn-species. In the cluster composed of two five-membered rings, a Zn^{2+} cation was placed (i) in the conventional ion-exchange site with two Al atoms in the same ring, (ii) in the same extra-framework site, but with only one Al atom in the same ring, the second Al atom being located in a neighboring ring. A third configuration (iii) consists of two Zn atoms close to the center of two edge-sharing five-membered rings containing each one Al atom, connected through a bridging O atoms to form a $[Zn—O—Zn]^{2+}$ particle. For dehydrogenation at an isolated Zn^{2+} cation, the rate-limiting step is the elimination of a hydrogen molecule with an intrinsic activation energy of 147 kJ/mol. Dehydrogenation over a $[Zn—O—Zn]^{2+}$ particle leads to a lower activation energy for the heterolytic dissociation, but to a very unfavorable intrinsic activation energy of 190 kJ/mol for direct ethene desorption and an even higher barrier 253 kJ/mol for H_2 elimination. Very recently Aleksandrov and Vayssilov [22] presented a similar cluster study of the dehydrogenation of ethane comparing the relative activity of three different types of Zn-cations: a Zn^{2+} cation in the vicinity of two Al atoms in a five-membered ring (similar to one of the configurations studied by Pidko and van Santen [21]), and $ZnOH^+$ and ZnH^+ in the vicinity of an isolated Al site. In addition to the two reaction mechanisms studied by Pidko and van Santen, a third scenario consisting of a simultaneous interaction of both methyl groups with the Zn^{2+} cation and a framework oxygen was proposed. Dehydrogenation over an isolated Zn-cation was found to be favored, with activation energies comparable to those quoted by Pidko and van Santen. However, while Pidko and van Santen concluded that after C—H bond-cleavage the most favorable proton accepting site was an oxygen atom in a neighboring ring, Aleksandrov and Vayssilov concluded that the lowest activation energy is found for a Zn^{2+} cation with two Al atoms in the same ring. In both studies, thermal effects were treated within harmonic transition state theory. While Pidko and van Santen[21] concentrated on the analysis of the vibrational eigenstates in relation to the experimental results available from infrared spectroscopy[7,13], Aleksandrov and Vayssilov[22] concentrated on the temperature dependence of the free energies of activation and suggested that entropy effects might at sufficiently high temperature reverse the energetic order of different reaction scenarios.

In this work, we present the results of an ab initio density-functional-based modeling study of the dehydrogenation of propane over Zn^{2+}-exchanged mordenite. Corrections for dispersion interactions not accounted for by density-functional theory have been considered. Our approach is based on a periodic model for the structure of the zeolite consisting of a unit cell doubled along the *c*-direction. Our active site is a bare Zn^{2+} cation residing in the conventional ion-exchange α-site, which is the most stable location of the Zn^{2+} cation in the main channel of mordenite [40]. The optimization of the structure of the adsorbate/zeolite complex is performed without any constraints, i.e. our approach accounts correctly for the flexibility of the zeolitic framework. The use of a large supercell allows achieving a realistic Al/Si ratio and also eliminates any possible interactions of the molecule with replicas in the neighboring cells. Transition states along the reaction have been determined as saddle points on the potential-energy surface. To permit a comparison with the earlier studies based on clusters, two cluster calculations have been performed, one using a large cluster surrounding the active site used in the periodic calculations, and a second based on the small cluster used by Pidko and van Santen [21]. This comparison highlights the important influence of the flexibility of the zeolitic framework on the activation energies for different steps of the reaction.

Entropy-effects have been considered at two different levels of theory: (i) within a harmonic transition state theory and (ii) using thermodynamic integrations based on free-energy gradients determined for a series of states along the transition path using constrained ab initio molecule-dynamics simulations. The thermodynamic integration allows to account for contributions to the entropy arising from very soft eigenmodes which are not adequately described within a harmonic approximation. Reaction rates can be calculated using an Arrhenius equation using the free energies of activation calculated within harmonic transition state theory, or derived from the ab initio thermodynamic integration. This analysis demonstrates the important role of anharmonic interactions in the various steps of the reaction.

2. Computational methodology

2.1. Density-functional calculations and dispersion corrections

Calculations are performed with the VASP code [23–26]. The density-functional calculations use the gradient-corrected functional PW91 [27,28]. The valence-core interaction is described within the all-electron projector-augmented wave (PAW) method [29,30] and valence orbitals are expanded in a plane-wave basis set. Brillouin-zone sampling is restricted to the Γ-point. The total-energy convergence is improved by a modest Gaussian smearing (0.1 eV) of the eigenvalues, total energies have been extrapolated to zero smearing.

Static total energy calculations for geometry optimization and transition state search use high-precision total-energy calculations with a plane-wave cutoff of 400 eV and standard precision of pseudopotentials (hard potentials). The full relaxation of atomic positions using the conjugate-gradient algorithm applies a stopping criterion of 10^{-5} eV for the self-consistency loop and of 10^{-4} eV for the geometry optimizer.

Because it is well known that DFT calculations underestimate the adsorption energies of saturated hydrocarbons in zeolites, dispersion corrections are calculated according to Grimme [32]. The dispersion-corrected total energy is given

$$E_{\mathrm{DFT-D}} = E_{\mathrm{KS-DFT}} + E_{\mathrm{disp}}, \tag{1}$$

where the dispersion corrections are described by semi-empirical pair potentials given for periodic systems by

$$E_{\mathrm{disp}} = -s_6 \sum_{i=1}^{N_{at}} \sum_{j=1}^{N_{at}} {\sum_{L}}' \frac{C_6^{ij}}{|r^{i,0} - r^{j,L}|^6} f(|r^{i,0} - r^{j,L}|), \tag{2}$$

where summations go over atoms N_{at} and all translations of the unit cell $L = (l_1, l_2, l_3)$, the prime indicates that $i \neq j$ for $L = 0$, s_6 is a global scaling factor, C_6^{ij} denotes dispersion coefficient for atom pair ij, $r^{i,L}$ is a position vector of atom i after performing L translations of the unit cell along lattice vectors. The term $f(r^{ij})$ is a damping function whose role is to scale the force field such as to minimize contributions from interactions within typical bonding distances. All force field parameters were set as proposed in Ref. [32] for the PBE functional. These parameters also apply to DFT calculations with the PW91 functional, because both functional produce very similar total energies.

2.2. Free energies of activation and reaction rates

The static transition state search uses the dimer method developed by Heyden et al. [31]. Adsorption and transition state energies are calculated as the difference of the total energies of the propane/zeolite complex from the static relaxation and the energies of the gas-phase molecule and the zeolite

$$E_{\mathrm{ads}} = E_{\mathrm{zeo+propane}} - E_{\mathrm{zeo}} - E_{\mathrm{propane}}, \tag{3}$$

intrinsic activation energies are calculated as the energy difference between reactants and transition states.

Within harmonic transition state theory (hTST), the reaction rate constant for each step is given by

$$k = \frac{k_B T}{h} \cdot e^{\frac{-\Delta F^h}{RT}} \tag{4}$$

with the free energy of activation given in the harmonic approximation by $\Delta F^h = \Delta E_{ZPE} + \Delta F^h_{vibr}$ and where ΔE_{ZPE} is the static activation energy corrected for zero-point vibrations and $\Delta F^h_{vibr} = -RTln(q_{TS}/q_{ini})$ the vibrational free energy calculated in the harmonic approximation from the partition function q_{ini} and q_{TS} of the initial and transition states.

Beyond the harmonic approximation, the change in the free energy between the initial and the transition state of an activated process can be calculated as a path integral over the free-energy gradient $\left(\frac{\partial F}{\partial \xi}\right)$ along the reaction coordinate ξ connecting the two stationary states [33]

$$\Delta F_{1\to 2} = \int_{\xi(1)}^{\xi(2)} d\xi \left(\frac{\partial F}{\partial \xi}\right)_{\xi^*}. \tag{5}$$

The free-energy gradient $\left(\frac{\partial F}{\partial \xi}\right)_{\xi^*}$ is evaluated at fixed values of the reaction coordinate ξ^* using constrained molecular dynamics simulations [34,35]. A detailed description of thermodynamic integrations applied to proton exchange reactions of hydrocarbon molecules over an acidic zeolite has been given by Bučko et al. [36]. Ensembles averages are taken over 6 ps, from MD runs performed at fixed cell volume and using a time-step of 2 fs. Soft pseudopotentials for O and N atoms allowing for a low energy cutoff of 200 eV have been used, and a 10^{-4} eV convergence criterion has been applied for stopping the SCF loop. In previous work [36] we have shown that in MD simulations cutoff energy may be reduced and convergence criteria relaxed without affecting the accuracy of the calculated ensemble average. The constant-temperature simulations apply the Verlet velocity algorithm [37], the temperature is controlled by an Anderson thermostat [38]. The reaction coordinate is described by a collective variable constructed as a combination of interatomic distances in a way that it is simple, complete, smooth, reversible, and imposes only soft restrictions on atomic movements [39], for details see below.

If the free energy of activation is decomposed according to $\Delta F = \Delta E + \Delta F_{vibr}$ into the energy of activation ΔE from the static potential-energy calculation, and the change in the vibrational contributions to the free energy ΔF_{vibr}, the importance of the anharmonic corrections can be assessed by the comparison of ΔF_{vibr} and ΔF^h_{vibr}. ΔF_{vibr} is temperature-dependent and determines a temperature-dependent reaction rate via Eq. (4) with a temperature-independent prefactor. Experimental activation energies E_a are usually assumed to be temperature-independent, they are derived from the reaction rate k measured at different temperatures via an Arrhenius relation of the form

$$k = A \cdot e^{\frac{E_a}{RT}} \tag{6}$$

and determined from a plot of ln k vs $1/T$. The free energy of activation may be decomposed into the enthalpy and entropy of the activation using the Eyring–Polanyi equation [46,47]

$$\ln\frac{k}{T} = \frac{-\Delta H}{R}\cdot\frac{1}{T} + \ln\left(\frac{k_B}{h}\right) + \frac{\Delta S}{R}. \tag{7}$$

3. Structure model and reaction scenario

The framework and the channel system of mordenite, as well as the location of the Zn^{2+} cation are displayed in Fig. 1. The lattice parameters are fixed to the values optimized by the DFT calculations of Demuth et al. [41] ($a = b = 13.655$ Å, $c = 7.606$ Å). All calculations are performed for the $1 \times 1 \times 2$ supercell shown in Fig. 1b. In the cell doubled in the c-direction the length of the main channel of ~15.2 Å is long enough to accommodate a linear hydrocarbon molecule. Moreover, the more isotropic shape of the supercell compared with the flat unit cell improves the stability of constrained MD simulations. The extra-framework Zn^{2+} cation compensates the negative charges of two framework Al/Si substitutions. A comprehensive analysis of the stability of Al/Si substitutions and the locations of extra-framework Zn^{2+} cations has been presented in our earlier work[40]. It has been demonstrated that for an isolated Al/Si substitution, a location in the T_2 tetrahedral site is most, and that in a T_4 site is least stable, in agreement with experimental results [42,44]. Placing one Al in a T_2 site and a second Al atom in all possible tetrahedral sites led to the following conclusions: (i) Location of Al in a T_4 site is energetically disfavored, as for single Al/Si substitutions. (ii) Two Al atoms in nearest-neighbor tetrahedral sites are energetically unfavorable, in agreement with Löwensteins rule [43]. (iii) Al/Si substitutions at short distances (in second-neighbor tetrahedral sites) are energetically slightly favored. This result is surprising, because it predicts a high stability for configurations with two Al atoms in the same small five- or six-membered ring, in contradiction to the "five-ring avoidance rule" formulated by Takaishi et al. [42] to explain the Al distributions derived from the Si NMR spectra. It was suggested

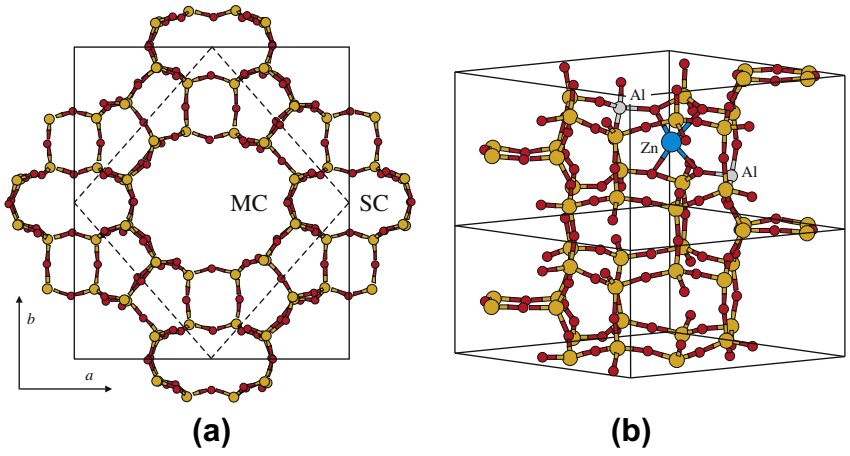

Fig. 1. Framework of mordenite projected along the c vector (a). The main channel (MC) and the side channel (SC). Full (dashed) lines indicate orthorhombic (monoclinic) unit cell. The monoclinic $1 \times 1 \times 2$ supercell (b). The active site is the Zn atom compensating two Al substitutions in the six-membered ring of the MC.

that the origin of this rule is not so much the energetics of the Al distributions but the preferential interaction of the functional groups of the structure-directing agents used in zeolite synthesis with more ionic Al atoms. Electrostatic effects result in larger Al—Al distances such that in low-Al zeolites the existence of Al—Si—Al sequences will be rather unlikely.

If a Zn^{2+} cation is placed into an extra-framework site, the energetically most favorable configurations were again found for the cation placed into the center of a five- or six-membered ring containing two Al atoms. However, analysis of the adsorption of molecular hydrogen demonstrated that the energetically most favorable configurations are also those with the lowest adsorption energies and only a modest degree of activation of the H—H bond. Dissociative adsorption (leading to the formation of a $[Zn—H]^+$ cation and a Brønsted OH group) was found to be always exothermic, with a more negative heat of adsorption if the Al atoms were placed at large distances. However, there were also some significant exceptions in the general trend. For a configuration with an Al atom in a T_2 site in a five-membered ring and the Zn^{2+} cation close to the center of this ring, the dissociation was only very weakly exothermic because the formation of a hydroxyl group is energetically unfavorable on framework oxygens connected to the extra-framework cation. A similar picture was derived for the dissociative adsorption of methane and the formation of a $[Zn—CH_3]^+$ cation and a Brønsted site. This agrees with the finding of Pidko and van Santen[21] that for the dehydrogenation of ethane adsorbed on a Zn^{2+} Lewis site, a location of the proton on an oxygen atom in the same ring is energetically less favorable than on an oxygen atom in a neighboring ring.

In our present work, we have decided to chose a configuration which (i) allows contact with larger molecules placed into the main channel of MOR, (ii) accounts for the "five-ring avoidance rule" of Takaishi et al. [42], (iii) allows to place both Al atoms into the same ring (thus creating an energetically favorable configuration), and (iv) has two "activated" oxygen atoms (i.e. atoms with Al nearest neighbors) in the same ring which are not connected to the Zn^{2+} cation and hence can act as proton-accepting sites. Such a configuration consists of two Al atoms in opposite corners of a six-membered ring (in one T_2 and one T_1 site) and a highly symmetric location of the extra-framework Zn^{2+} cation in the center of the ring (cf. Fig. 1b), forming a stable configuration [40]. Due to energetically favorable locations of both Al/Si substitution sites and the cation, this configuration is expected to occur frequently in mordenite.

The dehydrogenation of propane in the gas-phase is an endothermic reaction with a measured enthalpy of reaction of 124.9 ± 2.1 kJ/mol [45], to be compared with 153.2 kJ/mol resulting from DFT calculations. The reactions catalyzed by a Zn-exchanged zeolite proceeds in four steps, adsorption, dissociation and formation of a Zn-propyl and a Brønsted site, dehydrogenation, and desorption of propene according to the scheme:

$$MOR—Zn + C_3H_8 \rightarrow MOR—Zn\cdots C_3H_8, \quad (8)$$

$$MOR—Zn\cdots C_3H_8 \rightarrow H—MOR—Zn—C_3H_7, \quad (9)$$

$$H—MOR—Zn—C_3H_7 \rightarrow MOR—Zn\cdots C_3H_6 + H_2, \quad (10)$$

$$MOR—Zn\cdots C_3H_6 \rightarrow MOR—Zn + C_3H_6. \quad (11)$$

Alternatively to the dehydrogenation by reaction between the acid proton and a β-H atom of the chemisorbed propyl, a reaction scenario consisting of the elimination of propene from the Zn-propyl species, formation of a zinc hydride, followed by the recombinative desorption of a hydrogen molecule formed from the Zn-hydride and the Brønsted acid proton has been proposed [21]. Reactants, intermediates and products corresponding to reaction scenario (Eqs. (8)–(11)) are displayed in Fig. 2. Adsorption of propane occurs by formation of a contact between a terminal C atom and the Zn^{2+} cation (Fig. 2A) with a C-Zn distance of ~2.38 Å. After dissociation of a H atom from the terminal methyl group, the C—Zn distance is reduced to ~1.96 Å (Fig. 2B), reflecting a stronger binding of the propyl anion. The proton binds to an activated O atom of the zeolite framework next to the Al atom, forming a Brønsted acid site (Fig. 2B). Note that the acid proton binds preferentially to a O atom to which the Zn^{2+} cation is not connected. The acid proton attacks a β-H atom of the grafted propyl fragment

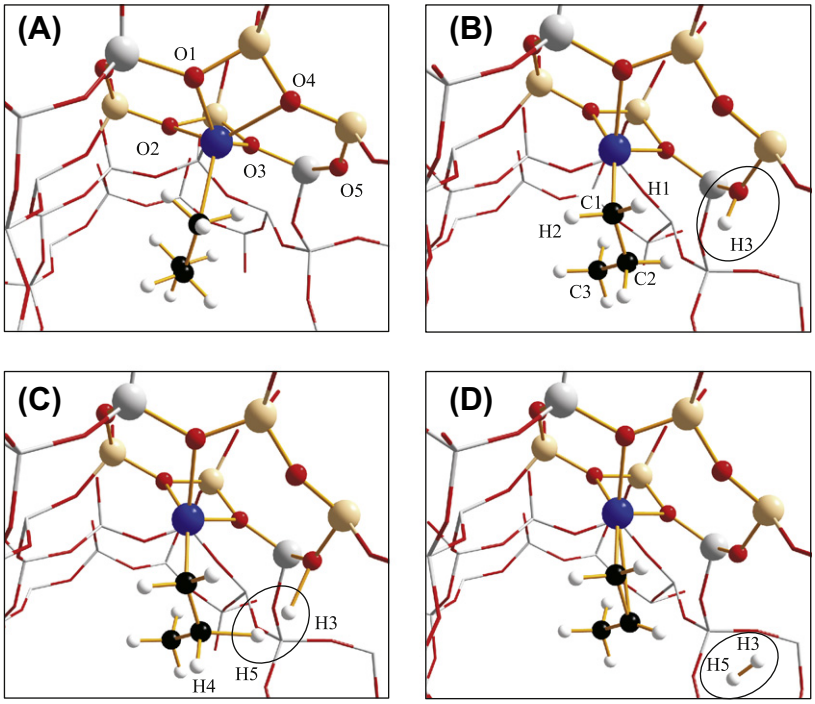

Fig. 2. Configurations along the reaction path for propane dehydrogenation. (A) Propane adsorbed on Zn^{2+}, (B) propyl bound to the Zn^{2+} cation and a Brønsted acid site (encircled), (C) an attack of the acid proton at a β-H atom of propyl , and (D) propene adsorbed on Zn^{2+} and a free H_2 molecule in the zeolite channel.

(Fig. 2C), forming a H_2 molecule while the propene molecule remains adsorbed on the Zn^{2+} cation (Fig. 2D).

4. Results and discussion

4.1. Reaction path – static periodic calculations

The activation energy for each reaction step is determined by the difference between the saddle-point energy and the total energy of the reactants. For the search of the saddle point along the reaction path, an appropriate reaction variable has to be defined. For the first reaction step, the abstraction of a H atom from propane adsorbed at the Zn-cation, the reaction coordinate may be defined as $\xi = r_1 - r_2$ where r_1 is the distance between the H-atom and the C carbon in the terminal CH_3 group and r_2 the distance between the H atoms and an "activated" O atom next to a Al/Si substitution site, i.e in the newly created Brønsted site (see Fig. 3a). For the second step, the formation of a H_2 molecule by reaction of the acid proton with a H atom from the propyl adsorbed at the Zn^{2+} cation, a convenient choice of a simple reaction coordinate is $\xi = r_1 + r_2 - r_3$ where r_1 is the C—H bond-length, r_2 the O—H bond-length and r_3 is the distance between the two H atoms forming the hydrogen molecule formed during the reaction (see Fig. 3b). The reaction coordinates involve the positions of all the atoms whose bonding is affected by the reaction; hence, it is complete and varies smoothly along the reaction path. The transition states along the reaction path are determined using Heyden's dimer method [31]. The same reaction coordinates have also been used in the thermodynamic integrations.

The potential-energy profile resulting from the static optimization of reactant, intermediate, and product configurations and the transition state search using the improved dimer method is displayed in Fig. 4 for DFT with and without dispersion corrections. Propane adsorption has been modeled in two steps: first, the molecule is placed approximately in the center of the main channel, then it is allowed to react with the Zn^{2+} cation. Long-range interactions of the saturated hydrocarbon with the zeolite framework are weak, propane in the main channel of MOR has an adsorption energy of only ~ -10 kJ/mol. Binding to the Zn^{2+} cation lowers the energy by ~ 60 kJ/mol, resulting in an adsorption energy of $E_{ads} \sim -70$ kJ/mol. Dissociation of propane into a propyl anion with a formal charge of -1bound to the Zn^{2+} cation and a proton forming a Brønsted acid site by binding to an activated O framework atom (configuration B) is weakly endothermic with a heat of reaction of

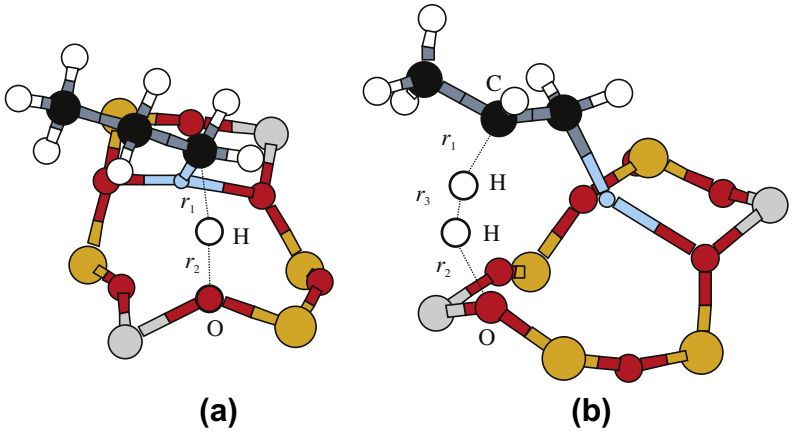

Fig. 3. Reaction coordinates $\xi = r_1 - r_2$ for the abstraction of a H atom from adsorbed propane (a) and $\xi = r_1 + r_2 - r_3$ for the formation of a hydrogen molecule by the reaction of a H atom of the adsorbed propyl and from the OH group of the Brønsted acid site (b), cf. text.

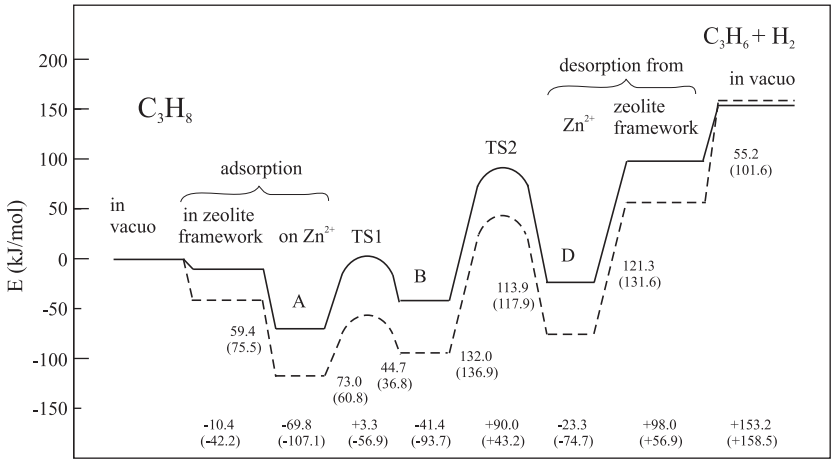

Fig. 4. Potential-energy profile for the dehydrogenation of propane as derived from static periodic calculations. The total energies E_{DFT} (in kJ/mol) are calculated relative to Zn—MOR and propane in the gas-phase. The configurations A (reactant–propane adsorbed at the Zn-cation in MOR), B and D (reaction intermediates) are same as in Fig. 2. Intrinsic activations energies for forward and backward reactions are listed on both sides of the transition states (TS1, TS2), adsorption (desorption) energies are decomposed into contributions from the binding to the Zn-cation and from the potential in the center of the zeolitic cavity. Dispersion-corrected total and activation energies E_{DFT-D} (Eq. (1)) are given in parentheses and displayed by dashed lines.

Table 1
Selected interatomic distances (in Å) of the intermediates and transition states for the dehydrogenation of propane over Zn^{2+}—MOR. Oxygen atoms binding the Zn^{2+} cation are labeled O1–O4, atoms located at opposite corners of the six-membered rings available for the formation of a Brønsted site O5 and O6. Hydrogen atoms in the terminal methyl groups are labeled H1–H3, those belonging to the secondary CH_2 group H4 and H5. $r_{1,2}$ and r_3 are the interatomic distances determining the reaction coordinates for the hydrogen-dissociation reaction ($\xi_1 = r_1 - r_2$) and for the formation of a hydrogen molecule ($\xi_2 = r_1 + r_2 - r_3$). Cf. Fig. 2 and text.

State		A	TS1	B	TS2	D
Zn—O1		2.036	2.065	2.084	2.060	1.995
Zn—O2		2.273	2.096	2.276	2.323	3.332
Zn—O3		2.018	2.217	2.393	2.060	2.042
Zn—O4		2.198	3.013	3.047	2.802	3.116
Zn—C1		2.318	2.065	1.956	2.017	2.173
C1—H1		1.097	1.104	1.101	1.098	1.095
C1—H2		1.118	1.114	1.100	1.100	1.094
C1—H3	r_1	1.118	1.483	3.809	2.996	3.442
O5—H3	r_2	3.118	1.248	0.979	1.568	3.685
C1—C2		1.549	1.538	1.533	1.438	1.369
C2—H4		1.099	1.102	1.103	1.095	1.097
C2—H5		1.100	1.099	1.105	1.525	3.223
H3—H5	r_3	2.423	2.309	2.356	0.839	0.750
ξ_1		−2.00	0.235	2.830		
ξ_2				1.632	3.725	6.377

∼28 kJ/mol and an activation energy of 73 kJ/mol, i.e. slightly higher than the desorption energy. The barrier of the inverse reaction is only 45 kJ/mol.

Geometric information on intermediates and transition states is compiled in Table 1. In the molecularly adsorbed configuration, all four bonds between the Zn^{2+} cation and framework oxygen atoms are preserved, C—H bonds in the terminal methyl group linked to the cation are slightly elongated (this is also reflected in a red-shift of the asymmetric C—H stretching mode – see below). In the transition state for dehydrogenation (TS1), one of the Zn—O bonds is broken and the H3 atom begins to connect to the activated framework oxygen O5. The contraction of the Zn—C1 distance shows that in the transition state the propane is more strongly attached to the cation than in the reactant state. Comparison of the C1—H3 and O5—H3 distances shows that this is a late transition state. In the intermediate state B, the short Zn—C1 distance reflects the strong binding in the $[Zn\text{-propyl}]^+$ complex. For the reaction intermediates (states B and D), as well in the transition state TS2 for the formation of a H_2 molecule the bond between the Zn^{2+} and the framework oxygen atom O4 is broken, reflecting the stronger adsorbate-cation and weaker cation-framework bonding. The C1—C2 distance shortens from ∼1.53 Å in propyl (state B) to ∼1.44 Å indicating a transition from a single C—C to a double C=C bond. The distance of two H atoms forming the H_2 molecule is 0.839 Å (cf. Table 1). The state D consists of propene adsorbed at the Zn^{2+} cation and a H_2 molecule in the cavity of the zeolite. While propane and propyl form a σ-bond to the Zn-cation, propene is adsorbed via the interaction of the π-states in the C=C bond with the cation. Two Zn—C distances of ∼2.17–2.48 indicate an asymmetric configuration of the adsorbed molecule.

The activation energy for the formation of a hydrogen molecule by reaction between the acid proton and a β-H atom of the propyl (transition state TS2) is ∼132 kJ/mol, this reaction is slightly endothermic with a heat of reaction of ∼18 kJ/mol. The activation energy for the reverse reaction is ∼114 kJ/mol. The energy difference between adsorbed propane and propene (plus a hydrogen molecule) is only ∼46 kJ/mol, i.e. much lower than the heat of reaction for dehydrogenation in the gas-phase. To desorb the propene molecule from the Lewis site requires an energy of ∼121 kJ/mol, further 55 kJ/mol are required to remove the propene and hydrogen molecules from the zeolite cavity.

4.1.1. Dispersion corrections to the potential-energy profile

The dispersion-corrected total energies along the reaction path are shown in Fig. 4 as dashed lines, numerical values are given in parentheses. Van der Waals forces increase the adsorption energy of propane placed into the center of the zeolitic cavity by −31.8 kJ/mol to −42.2 kJ/mol, the energy of chemisorption at the Zn^{2+} cation increases by 37.3–107.1 kJ/mol. As the transition state TS1 is less strongly stabilized by the dispersion forces, the activation energy is reduced by about 12 kJ/mol to ∼61 kJ/mol. Hence, dispersion corrections make an important difference: while without van der Waals corrections the desorption energy of propane is lower than the activation energy for heterolytic dissociation of a H atom, the situation is reversed if the dispersion corrections are taken into account. If only the energy required to detach propane from the Lewis site (without eliminating it from the zeolite) is considered, the impact of the dispersion forces is even more pronounced. The dispersion corrections are also smaller for the covalently-bonded Zn-propyl species such that the reaction is now slightly less endothermic. For the second reaction step, the abstraction of a hydrogen molecule, the dispersion corrections are essentially thermo-neutral, the endothermic heat of reaction is increased only by 1 kJ/mol. The effect of the van der Waals forces is only slightly more pronounced for the transition state TS2, the activation energy increases from 132 kJ/mol to 137 kJ/mol. Hence, the most important contribution of the dispersion forces is to stabilize the adsorption of the saturated alkane at the Lewis site, followed by a reduction of the activation energy for dissociation.

4.2. Reaction path – static cluster calculations

It appears to be tempting to compare the present results for the dehydrogenation of propane with those of the previous cluster studies for the dehydrogenation of ethane [21,22]. However, not only the difference in the length of the alkane and the different description of the zeolite (large periodic model vs. minimal cluster) has to be considered, the studies differ also in the configurations chosen for the Lewis site and in the choice of the exchange-correlation functional (Aleksandrov and Vayssilov[22] used a conventional, although slightly different gradient-corrected functional, whereas Pidko and van Santen [21] used a hybrid functional). To permit a serious assessment of the differences between periodic an cluster calculations, the potential-energy profile for the dehydrogenation of propane by Zn—MOR was calculated for two types of clusters: (i) A large cluster consisting of a complete ring surrounding the zeolitic cavity and the Zn-cation located in a six-membered ring with two Al/Si substitutions, in exact correspondence to our periodic model. This cluster contains 22 tetrahedral sites. (ii) A small cluster consisting of two edge-sharing five-membered rings with two Al/Si substitutions in one of the rings, in analogy to the cluster used by Pidko and van Santen to study ethane dehydrogenation [21]. The two clusters are shown in Fig. 5.

The calculations have been performed for clusters placed into the center of a large periodically repeated box. The dimensions are 16 × 16 × 15 Å for the large cluster, the minimal distances between periodically repeated images of the clusters (between terminating H atoms whose positions are frozen) are 3.5–5 Å. The positions of the atoms in the cluster are initially the same as in the periodic structure, all dangling bonds were saturated with hydrogen and the Si—H and Al—H bond-lengths were optimized while the positions of all other atoms remained fixed at their crystallographic positions. For the study of the adsorption and dehydrogenation of propane, the positions of the terminal H atoms are fixed, while all other atomic coordinates are optimized. This corresponds to the procedure adopted by Pidko and van Santen. Dispersion corrections have not been considered, because for the small cluster no interactions of the molecule with the wall of the

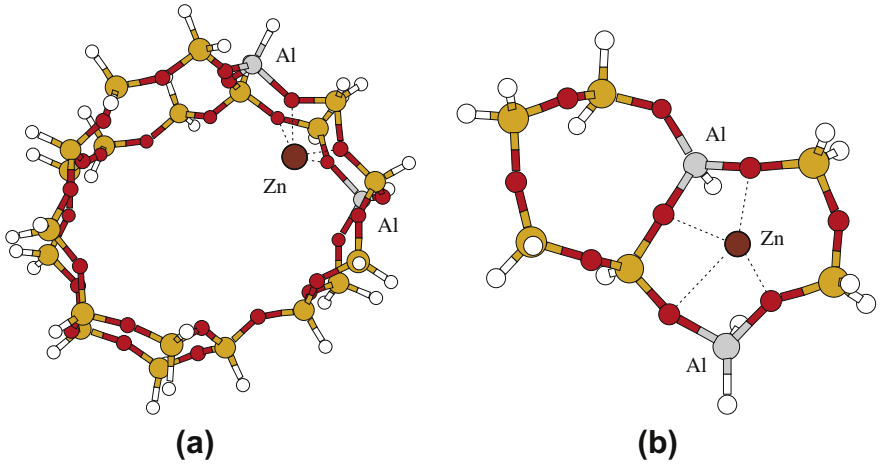

Fig. 5. Large (a) and small (b) cluster models for Zn—MOR, cf. text and Fig. 1 for the full periodic structure.

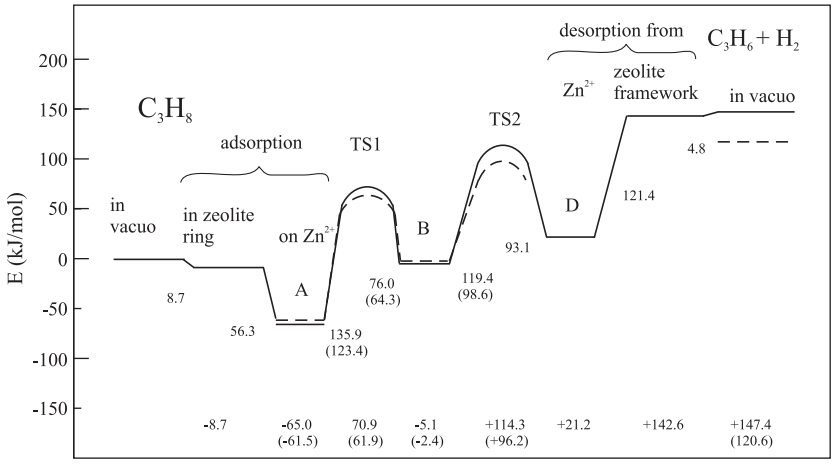

Fig. 6. Potential-energy profile for the dehydrogenation of propane as derived from DFT calculations for the large cluster. The total energies E_{DFT} (in kJ/mol) are calculated relative to the isolated cluster and propane in the gas phase. The configurations A, B and D represent adsorbed propane (A), adsorbed propyl plus a Brønsted site (B), and adsorbed propene plus a free H_2 molecule (D). Intrinsic activations energies for forward and backward reactions are listed on both sides of the transition states (TS1, TS2). Zero-point corrected total and activation energies are given in parentheses and displayed by dashed lines.

zeolitic cavity are possible. The potential-energy profile for the dehydrogenation reaction, as calculated for the large cluster is shown in Fig. 6.

Compared to the periodic calculations, we find a good agreement for the adsorption energy of propane (which is lower by ~5 kJ/mol only), but a dramatic increase in the activation energy for H-dissociation (TS1) which is almost doubled compared to the periodic calculations (~136 kJ/mol vs. 73 kJ/mol). Likewise, the reaction intermediate B is destabilized, being only 5 kJ/mol below the reference energy. On the other hand, the activation energy for the formation of a hydrogen molecule by reaction between a β-H atom of propyl and the Brønsted H-atom (TS2) decreases to 119 kJ/mol (132 kJ/mol in the periodic calculations). The energy required to detach propene from the cation (~121 kJ/mol) is the same as calculated with the periodic model, but much more energy is required to eliminate propene from the cavity in the extended periodic structure than from the center of the ring-shaped large cluster.

The ZPE-corrected energies of configurations A and B only slightly differ from the static potential energies. Because in a transition state one vibrational frequency is imaginary and does not contribute to the partition function, the ZPE-correction is slightly larger for TS1 compared with configurations A and B. The ZPE-corrected energy decreases by ~7 kJ/mol and ~18 kJ/mol for TS1 and TS2, respectively. It is well known that the dehydrogenation has a significant effect on the calculated reaction enthalpy [48,49]. Upon the dehydrogenation of propane, the number of bonds decreases by one and the number of vibrational modes of a single molecule decreases by five. The cluster calculation of products in vacuo provides the ZPE-correction of ~27 kJ/mol and the over-all reaction enthalpy is 120.6 kJ/mol, in reasonable agreement with the experimental enthalpy measured in the gas phase of 124.9 ± 2.1 kJ/mol [45]. Due to numerical difficulties with the location of the global potential-energy minimum for the configuration D (the weakly bonded H_2 molecule can be located in numerous sites along the zeolite ring), the ZPE-correction is not calculated.

While the periodic calculations predict that the activation energy for H_2 elimination is much higher than for the heterolytic H-dissociation, the cluster calculations predict that the activation energies for H-dissociation from absorbed propane and H_2 elimination are of comparable magnitude. The origin of the differences in the reaction scenarios are evident: while for the weak interaction between the saturated propane molecule and the Zn-cation, cluster and periodic calculations are in good agreement, the stability of the more strongly bound intermediates (adsorbed propyl and propene) and of the transition states is drastically reduced in the cluster

models. The essential difference is the flexibility of the periodic framework of the zeolite which is absent due to geometric constraints imposed on the boundary of the cluster. However, in both cases, the activation energy for the reaction reversing the H-dissociation is much lower than for the forward reaction. This will reduce the concentration of the reaction intermediate B – a more detailed analysis would require a detailed micro-kinetic modeling. The over-all heat of reaction for the propane dissociation (propane → propene + H_2) is 154.4 kJ/mol (calculated for a gas-phase reaction), 153.2 kJ/mol (calculated using a periodic model of MOR) and 147.4 kJ/mol (calculated using the cluster model) – the small remaining differences reflect the margin of inaccuracy of the calculations. These are due to the fact that after going through the various reaction steps, the systems do not completely relax to their initial states.

A similar picture arises from the calculations using the small cluster with eight tetrahedral sites only (Fig. 7). In this case, we have studied a reaction path for the dehydrogenation of ethane where the Brønsted site was created in the five-membered ring centered by the Zn-cation. This permits a direct comparison with earlier cluster studies. The calculations follow the same strategy as for the large cluster with the Zn-cation in a six-membered ring. The adsorption energy of ethane is reduced because of the lower reactivity of a Zn-cation in close proximity to two Al atoms, but the activation energy for the heterolytic H-dissociation is only slightly higher than for the large cluster and much higher than calculated using the periodic model. The activation energy for the H_2 elimination is strongly increased to ~189 kJ/mol, which is much higher than found using both the periodic and the large cluster calculations. The reason is that the Brønsted proton placed into the same five-membered ring as the cation has lower acidity than the proton in the larger six-membered ring at a slightly larger distance from the Zn-cation. In the energetic profile, we have also included the activation and intermediate-state energies calculated by Pidko and van Santen [21] for ethane dehydrogenation. We find that the profiles are in semiquantitative agreement; hence, by comparison with the earlier cluster calculations for ethane dehydrogenation, we can draw some general conclusion regarding the dehydrogenation of short alkanes.

4.2.1. Comparison with cluster calculations for ethane dehydrogenation

We begin with the variation of the adsorption energy in the series methane–ethane–propane. For the same Lewis site configuration as used in the periodic calculations, the adsorption energies are −45/−50/−59 kJ/mol for methane/ethane/propane (without dispersion corrections). Aleksandrov and Vayssilov did not report adsorption energies, but Pidko and van Santen found adsorption energies of −26 kJ/mol for a Zn^{2+} cation with two Al sites in the five-membered ring and −53 kJ/mol if only one Al atom is located in the same ring. According to our previous work [40], sites with the Zn^{2+} cation in a five-membered ring have adsorption energies for methane of −44 kJ/mol if two Al atoms are present in the ring, increasing to −65 to −78 kJ/mol if only one Al is present in the ring. We did not extend these calculations to ethane, but the comparison suggests that the adsorption energies calculated by Pidko and van Santen [21] using a hybrid functional are lower than those calculated using a gradient-corrected functional by about 20 kJ/mol, in agreement with many similar observations. The difference between a cluster and a periodic approach is evidently less important at this point.

For the activation energy of the first reaction step (H-dissociation from ethane), Pidko and van Santen [21] calculated intrinsic activation energies of 117 and 150 kJ/mol for one Al atom in the 5MR, and of 139 and 168 kJ/mol for two Al atoms in the same 5MR as the Zn cation (the lower value always applies to the case where the Brønsted site is created in a different 5MR). The activation energy of 79 kJ/mol reported by Aleksandrov and Vayssilov[22] for a Zn-cation in the same 5MR with two Al sites is calculated relative to the ethane molecule in the gas-phase, i.e. the adsorption energy has to be added to allow comparison with the intrinsic activation energies. Assuming an adsorption energy of ~−50 kJ/mol comparable to our result (as suggested by the results for methane adsorption), an intrinsic activation energy of ~130 kJ/mol can be estimated. Hence, the difference in the functionals used by both cluster calculations seems to be less important for the activation energies than for the adsorption energies.

At this stage, we note an important difference between our results derived from periodic models on one hand, and our cluster

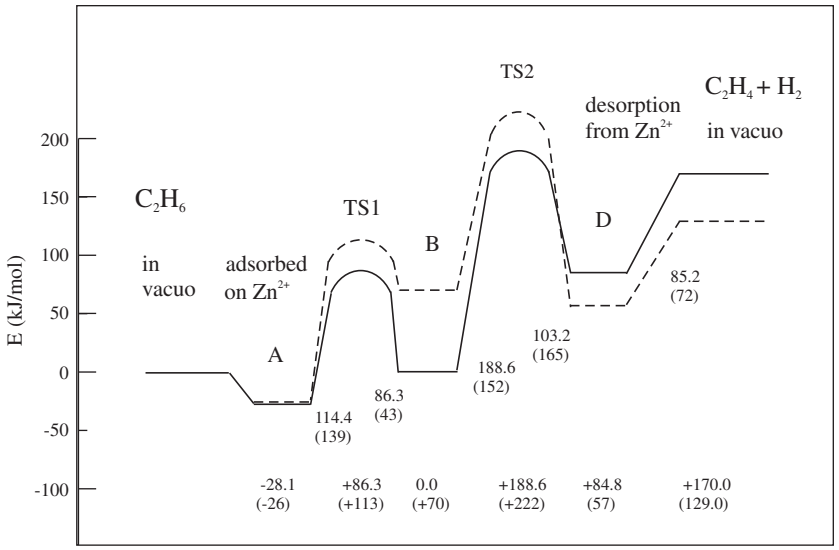

Fig. 7. Potential-energy profile for the dehydrogenation of ethane as derived from DFT calculation for the small cluster consisting of two five-membered rings only. The total energies E_{DFT} (in kJ/mol) are calculated relative to the isolated cluster and ethane in the gas-phase. The configurations A, B and D represent adsorbed ethane (A), adsorbed ethyl plus a Brønsted site (B), and adsorbed ethene plus a free H_2 molecule (D). Intrinsic activations energies for forward and backward reactions are listed on both sides of the transition states (TS1, TS2). Numbers in parentheses and dashed lines give the energies calculated for ethane dehydrogenation by Pidko and van Santen [21] using hybrid functional and the same cluster and reaction scenario.

results and those of the previous cluster studies on the other hand. The cluster calculations predict an intrinsic activation energy which is much higher than that from the periodic calculations (and further increased for a cation location in a five-membered instead of a six-membered ring). For the cluster calculations, the activation energy is always higher than the desorption energy of the reactant, while in our study we derived an activation energy which is comparable (or even lower, if dispersion corrections are taken into account) than the desorption energy. We think that the lower activation energy achieved in our calculations is the result of the full flexibility of the zeolitic framework – optimization of all configurations is performed without any other constraints other than the fixed volume and shape of the large supercell. Optimization of the clusters on the other hand is subject to various constraints fixing the boundary of the cluster.

For the activation energy of the H_2 elimination step Pidko and van Santen [21] reported values varying between 106 and 166 kJ/mol, depending on the location of the Al atoms and of the Brønsted site. The reaction is weakly exo- or endothermic, with the heat of reaction varying between −59 and +15 kJ/mol. Aleksandrov and Vayssilov [22] found a comparable activation energy of 154 kJ/mol for their cluster consisting of a single ring. We find here a similar activation energy of 132 kJ/mol for periodic and of 119 (189) kJ/mol using the large (small) cluster.

Hence, the decisive difference between the cluster calculations and our periodic simulations is in the activation energy for the dissociation step. We think that the difference arises (i) from a more appropriate choice of the active site which allows to accommodate both Al/Si substitution sites and the Brønsted site in the same six-membered ring without a significant energetic penalty and (ii) to the fact that our periodic simulations account for the full flexibility of the zeolitic framework. We expect that the scenario for the dehydrogenation of other short alkane will be similar to that described here for propane.

4.3. Harmonic transition state analysis

Vibrational frequencies of reactants, transition states and products have been calculated using the direct force-constant approach implemented in VASP. Knowledge of the eigenstates allows to estimate the entropic contributions to the reaction barriers and reaction rates, as well as to confront our results with experimental infrared spectroscopy.

4.3.1. Vibrational eigenstates of the adsorbate–substrate complex

Diffuse reflectance infrared Fourier transform (DRIFT) measurement have been presented by Kazansky et al. [13,17] for methane and ethane adsorbed on Zn-exchanged ZSM5. For adsorbed methane a very intense mode at 2805 cm^{-1} has been attributed to a strongly red-shifted symmetric C—H stretching mode. For adsorbed ethane a strongly red-shifted band at about 2738 cm^{-1}, a group of four modes in the range of 2875–2993 cm^{-1}, with relative intensities varying strongly with partial pressure and temperature treatment have been detected. After heating at moderate temperatures also the modes at 3610 cm^{-1} characteristic for OH groups appeared.

The calculated C—H stretching frequencies of propane adsorbed in the zeolite framework range between 2960 cm^{-1} and 3050 cm^{-1}. Upon adsorption on the Zn^{2+} cation the C—H stretching frequencies of two H atoms neighboring with the cation decrease to 2806 cm^{-1} and 2868 cm^{-1}. The red-shift by ∼150 cm^{-1} reasonably compares with red-shifted modes observed in IR spectra of methane and ethane [13,17]. No red-shifted modes are calculated for the chemisorbed configuration B. The stretching frequency of the hydroxyl group at the Brønsted site is 3660 cm^{-1}.

Table 2
Vibrational enthalpy H_{vib} and entropy S_{vib} of configurations along the reaction path, calculated at T = 300 K in the harmonic approximation.

Configuration	H_{vib} (J/mol)	S_{vib}(J/K mol)
A	393.8	184.8
TS1	377.3	161.3
B	391.4	186.9
TS2	369.4	165.6
D	373.8	217.6

Table 3
Static activation energy ΔE, activation energy corrected for zero-point energy ΔE_{ZPE}, entropy terms $T \cdot \Delta S$, and the change of the free energy ΔF_{hTST} (kJ/mol).

Transition	ΔE	ΔE_{ZPE}	$-T \cdot \Delta S$	ΔF_{hTST}
A → TS1	73.0	58.1	7.1 (300 K)	65.2
			12.5 (500 K)	70.6
			17.9 (700 K)	76.0
B → TS1	44.7	33.2	7.7 (300 K)	40.9
			15.4 (500 K)	48.6
			23.2 (700 K)	56.4
B → TS2	132.0	112.2	6.4 (300 K)	118.6
			11.2 (500 K)	123.4
			15.7 (700 K)	127.9
D → TS2	113.9	116.3	15.6 (300 K)	131.9
			31.4 (500 K)	147.7
			47.4 (700 K)	163.7

4.3.2. Free energies calculated in a harmonic approximation

The vibrational enthalpies and entropies calculated in the harmonic approximation at a modest temperature of 300 K for the reaction intermediates and transition states are compiled in Table 2. The important result is the variation of the entropy along the reaction path. In the transition state TS1 for heterolytic H-dissociation, the system looses entropy because of a sharply defined transition state geometry with the H3 atom in a position about half-way between the terminal C1 atom and the framework oxygen O5 (see Table 1). In the intermediate state B (adsorbed propyl), the entropy is again almost the same as for the reactant state (adsorbed propane). Entropy is decreased again in transition state TS2, but strongly increased in state D due to the high mobility of the H_2 molecule in the zeolitic cavity.

Table 3 compiles the zero-point corrected activation energies and the entropic contributions to the free energies of activation at different temperatures, calculated in the harmonic approximation. Fig. 8 presents the zero-point corrected potential-energy profile, with and without dispersion corrections. Zero-point corrections lead to an over-all reduction of the activations energies, the effect is strongest for the H_2 elimination step were the activation energy is reduced from 132 to 112 kJ/mol. The ZPE-corrected reaction enthalpy of 119.5 kJ/mol agrees with the reaction enthalpy calculated using the large cluster (cf. Fig. 6) of 120.6 kJ/mol and is in reasonably good agreement with the experimental gas-phase dehydrogenation enthalpy of propane of 124.9 ± 2.1 kJ/mol [45]. Entropic contributions lead to free-energy barriers which increase with temperature. This effect is largest for the inverse reaction D → TS2 because of the large loss of entropy compared to a configuration D where the H_2 molecule moves freely in the cavity of the zeolite.

4.4. Thermodynamic integrations

We have used thermodynamic integrations to calculate the change in the free energy between the reactant, transition, intermediate and product states determined by the static calculations.

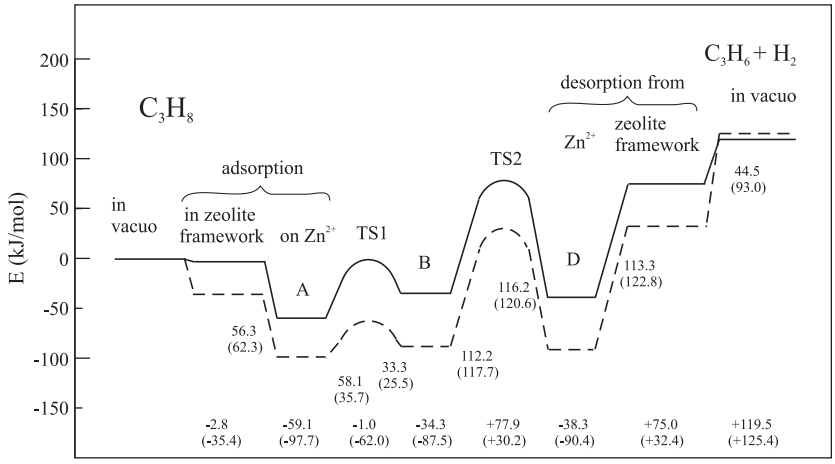

Fig. 8. Potential-energy profile for the dehydrogenation of propane as derived from periodic calculations, including zero-point calculations, without (full lines) and with dispersion corrections (broken lines and numbers in parentheses).

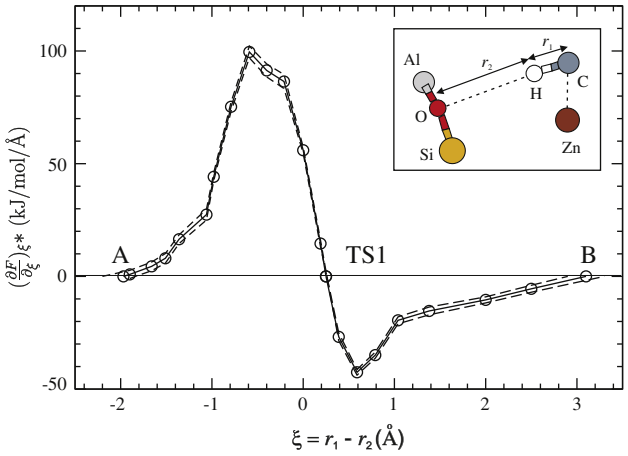

Fig. 9. Gradients of the free energy between configurations A and B (cf. Figs. 2 and 4) calculated at 300 K. Geometry parameters used to construct the collective variable ξ are shown in upset. Dashed lines show standard deviations.

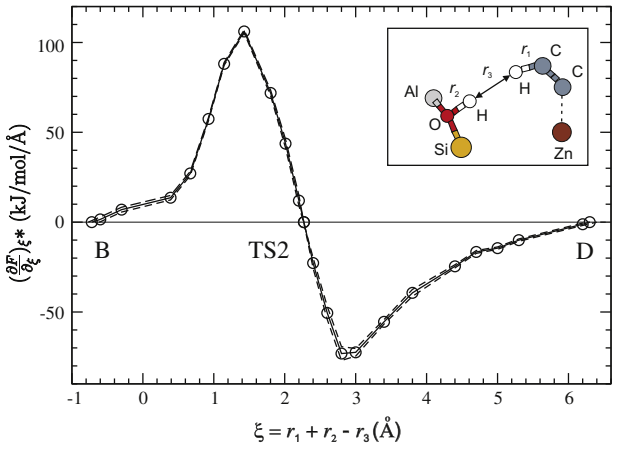

Fig. 10. Gradients of the free energy between configurations B and D (cf. Figs. 2 and 4) calculated at 300 K. Dashed lines show standard deviations.

The reaction coordinate connecting reactant and product states has been defined above.

4.4.1. Constrained MD – free energies of activation

The gradients of the free-energy change $\left(\frac{\partial F}{\partial \xi}\right)$ for the dissociation (A → B) calculated at 300 K are displayed in Fig. 9. During the dissociation, a change of bonding of three atoms C, H, and O occurs (cf. inset in Fig. 9). The constrained MD uses the collective variable $\xi = r_1 - r_2$ (cf. inset in Fig. 9). A continuous change of ξ leads to the conversion of the structure A to the transition state TS1 and further to the structure B, in which the Brønsted acid site is formed. The values of the collective reaction coordinate at 300 K (Fig. 9) are −1.97/0.25/3.1 Å for configurations A/TS1/B, respectively, only slightly different from the $T = 0$ K limit (cf. Table 1). In the transition state the H atom to be dissociated from propane is about half-way between the terminal C and the framework oxygen atom. Because of larger electronegativity and therefore larger attractive power of the O atom, the equilibrium position is shifted towards the C atom and at 300 K corresponds to $\xi = 0.25$ (cf. Fig. 9).

Fig. 10 displays the free-energy gradients calculated for the dehydrogenation of the reaction intermediate between structures B and D (cf. Figs. 2 and 4). Here, the change of bonding of four atoms occurs (C, 2H, and O). The simplest, complete, and smooth collective variable is $\xi = r_1 + r_2 - r_3$, where r_1 is the C—H bond-length, r_2 is the O—H bond length, and r_3 is the distance between two H atoms, which are extracted from the framework and the zinc-propyl intermediate, and form the H_2 molecule (cf. inset in Fig. 10).

Changes of the free energy calculated as a path integral (cf. Eq. (5)) between stationary points of the reaction coordinate A, TS1, B, TS2, and D (cf. Figs. 9 and 10) at 300 K, 500 K, and 700 K are collected in Table 4. Standard deviations of the free-energy changes are calculated via the integration of maximum/minimum values of the gradients allowed by the standard deviation in the MD run of the particular configuration. Note that for MD runs of the same length the standard deviation increases with increased temperature of the MD simulation.

The comparison of the free energies of activations from the full anharmonic approach and from the harmonic approximation demonstrates that the successive steps of the reaction are affected to a different degrees by anharmonic effects. The barrier for the heterolytic H-dissociation (A → TS1) is strongly increased – evidently this is a consequence of the loss of entropy during the activation from a weakly adsorbed propane molecule to a more strongly bound transition state. The geometric analysis has demonstrated that TS1 is a late transition state, the H atom abstracted from propane is already closer to the framework oxygen than to the terminal C atom. The

Table 4
Changes of the free energy calculated as a path integral of free-energy gradients between stationary points (ΔF_{anharm}) and in the harmonic approximations (ΔF_{harm}), in kJ/mol.

T	Transition	ΔF_{anharm}	ΔF_{harm}	Transition	ΔF_{anharm}	ΔF_{harm}
300 K	A → TS1	98.8 ± 5.0	65.2	B → TS1	42.9 ± 4.3	40.9
500 K		113.9 ± 6.4	70.6		51.2 ± 4.9	48.6
700 K		121.1 ± 7.6	76.0		52.0 ± 6.5	56.4
300 K	B → TS2	119.4 ± 3.9	118.6	D → TS2	119.1 ± 5.8	131.9
500 K		126.3 ± 6.4	123.4		140.1 ± 6.6	147.7
700 K		132.3 ± 7.4	127.9		151.1 ± 9.8	163.7

Table 5
Natural logarithms of reaction rates calculated using mean values of path-integrated free energies (s^{-1}).

T	Transition	ln$k$		Transition	ln$k$	
		Anharm	Harm		Anharm	Harm
300 K	A → TS1	−10.168	7.102	B → TS1	12.260	15.641
500 K		2.580	14.084		17.669	18.455
700 K		9.505	17.166		21.367	19.641
300 K	B → TS2	−18.421	−11.826	D → TS2	−18.290	−18.693
500 K		−0.404	0.680		−3.721	−1.835
700 K		7.573	9.487		4.353	9.828

transition state resembles already rather closely the intermediate state B (propyl adsorbed at the cation plus an OH group). This also explains that the reverse reaction (activation B → TS1) is hardly affected by anharmonic effects. Anharmonicity is strongest for the weakly bound adsorbed propane where the softest modes (vibrations and librations of the molecule relative to the framework) are not well described in an anharmonic approximation. The next activation step (B → TS2) is also hardly affected by anharmonicity because in both cases there are no soft modes in either configuration. The activation from the reverse reaction (D → TS2) is strongly affected by the anharmonic contributions because in state D (adsorbed propene plus a H_2 molecule in the cavity) the translational and rotational motions of the nearly free hydrogen molecule are not adequately described within a harmonic theory. Altogether we find that while within harmonic transition state theory, the rate-determining step for the dehydrogenation process is the H_2-elimination step, the thermodynamic integrations lead to a slightly different picture, with a smaller difference in the free energies of activation decreasing further at elevated temperatures.

The path-integrated free energies of activation may be decomposed into enthalpy and entropy contributions using the Eyring–Polanyi equation plots (cf. Eq. (7)). This analysis demonstrates that anharmonicity effects are strongest for the heterolytic dissociation (A → TS1) were the loss of entropy upon activation is −24 J/mol K in the harmonic approximation and −60 J/mol K from the thermodynamic integration: Anharmonicity also leads to a larger loss of entropy (−86 J/mol K instead of −52 J/mol K) for the D → TS2 activation, while the activation processes starting from the intermediate B are hardly affected.

4.5. Reaction rates

Reaction rates calculated according the Arrhenius equation (Eq. (6)), using the free energies of activation from the thermodynamic integrations (and including anharmonic effects) and from harmonic transition state theory are collected in Table 5.

The reaction rates are inversely proportional to the change of the free energy ΔF. At 300 K, the lowest rate resulting from the thermodynamic integrations is calculated for the H_2 elimination [B → TS2, ln k = −18.4 (−11.8) – reaction rates from harmonic transition state theory are given in parentheses] which is much slower than the heterolytic H-dissociation [A → TS1, ln k = −10.2 (7.1)]. Reaction rates calculated from hTST are much higher because the harmonic approach underrates the loss of entropy upon activation. If anharmonicity is taken into account not only rates are reduced, but the difference in the reaction rates of the two steps is also reduced. However, the concentration of the reaction intermediate (the Zn-propyl complex plus a Brønsted site) is also reduced by a very fast backward reaction (B → TS1) which is slowed down due to anharmonic effects. At higher temperature, the relative magnitudes of the reaction rates change appreciably. At 700 K, the reaction rates for the H-dissociation and H_2 elimination steps are comparable in the anharmonic approach, while in hTST the rate of H-dissociation is still much higher. However, as the rate for the reverse B → TS1 increased much faster with temperature in the anharmonic approach, the H-dissociation step remains dominant.

Experimental activation energies are usually derived from reaction rates measured at different temperatures and assuming a temperature-independent heat of activation E_{act} and an equally temperature-independent prefactor. We have used Arrhenius plots constructed according to Eq. (6) to derive effective activation energies from the reaction rates calculated using both harmonic TST and thermodynamic integrations. The analysis shows that although harmonic and anharmonic calculations yield prefactors differing only by up to about 20% of ln A, the effective activation energies derived from the Arrhenius plots can differ by up to a factor of two and reflect the different energy dependence of the harmonic and anharmonic free energies of activation. The effective activation energies derived from the reaction rates determined by thermodynamic integration are very close to the enthalpies of activation ΔH derived from the decomposition of the free energies using the Eyring–Polanyi equation. However, the effective activation energies determined via hTST are quite different from the zero-point corrected activation energies ΔE_{ZPE} derived from the static potential-energy profiles. The effective activation energies may be larger or smaller than the ΔE_{ZPE}, depending on the temperature dependence of the harmonic vibrational energies.

The largest difference in the effective activation energies is calculated for the heterolytic H-dissociation and the corresponding reverse reaction; in both cases, the anharmonic result is about two times larger than the harmonic result. Both activation processes are connected with a large loss of entropy which is underestimated in hTST and this is reflected in the much too low effective interaction energy. Differences are much more modest for the H_2 elimination and the reverse process.

5. Conclusions

The reaction path for the dehydrogenation of propane over Zn-exchanged mordenite has been investigated using ab initio density-functional calculations at different levels of theory: calculations for periodic models and finite clusters, calculations with and without corrections for dispersion forces, free energies of activation determined using harmonic transition state theory and using thermodynamic integrations based on constrained ab initio molecular dynamics.

For the location of the Zn^{2+} cation, we have chosen a configuration which (i) allows a contact between the cation and larger molecules placed into the main channel of the zeolite, (ii) is energetically sufficiently favorable to occur with high probability, (iii) accounts for the "five-ring avoidance rule", and (iv) has two activated framework oxygen atoms at close distances not connected to the Zn^{2+} cation which favor the formation of a Brønsted site. Such a configuration is realized for an α-site with two Al/Si

substitution at opposite corners of a six-membered ring at the side wall of the main channel and the Zn^{2+} cation in the center of the ring.

Calculations of the static activation energies of the reaction via the improved dimer method have been performed using a large periodic model with a computational cell consisting of two unit cells of mordenite, and for a large and a small cluster model. The large cluster with 22 tetrahedral sites is chosen such that the cluster encloses the main channel of mordenite, the small cluster with eight tetrahedral sites consists of two edge-sharing five-membered rings. This smaller cluster is identical to that used in earlier studies of the dehydrogenation of ethane [21].

The reaction proceeds via (i) physisorption of propane at the Zn^{2+} cation, (ii) dissociation of a H-atom leading to the formation of chemisorbed propyl and a Brønsted site, (ii) dehydrogenation via the recombinative desorption of a hydrogen molecule from the chemisorbed propyl and the Brønsted site, and (iv) desorption of propene.

The periodic calculations without dispersion corrections, but including zero-point corrections yield an adsorption energy for propane of −59 kJ/mol, activation energies of 58 kJ/mol and 112 kJ/mol for the dissociation and dehydrogenation steps and a desorption energy for propene of 158 kJ/mol. Dispersion corrections increase the adsorption energy of propane to −98 kJ/mole and the desorption energy of propene to 216 kJ/mol, but reduce the activation energy for hydrogen dissociation to 36 kJ/mol and increase the activation energy for dehydrogenation only slightly to 118 kJ/mol. Hence, the most important effect of the dispersion corrections is to stabilize physisorbed propane – only with these corrections the activation energy for H-dissociation is just a bit lower than the desorption energy of propane. However, for the H-dissociation the barrier for the reverse reaction (33 kJ/mol and 26 kJ/mol without and with dispersion corrections, respectively) is much lower than for the forward direction, leading to a low concentration of the reaction intermediate B. For the H_2 elimination step, the barriers for forward and backward reactions are comparable.

The reaction scenario resulting from the cluster calculations is different. Zero-point corrected calculations for the large cluster produce an activation energy for the H-dissociation step which is with 123 kJ/mol now higher than that for the dehydrogenation step with 96 kJ/mol (no dispersion corrections are considered). The cluster calculations also account only for that part of the adsorption/desorption energies of propane and propene which are due to the interaction with the Lewis acid site, but not of the stabilizing contribution of the zeolitic framework. Therefore, a comparison of desorption energies is not very meaningful – it would only lead to the conclusion that desorption is strongly preferred over H-dissociation. The decisive difference between the periodic and the cluster calculations is that the former account for the flexibility of the zeolitic framework, while for a finite cluster the possibility to react to the perturbation created by the adsorbate is strongly limited by the constraints necessarily imposed to its boundary.

Reaction rates have been calculated within harmonic transition state theory and via free energies of activation calculated by thermodynamic integrations. Free energies of activation for the H-dissociation step are much lower if calculated using hTST ($\Delta F_{harm}(A \rightarrow TS1) \sim 65$ kJ/mol at 300 K) than derived from thermodynamic integrations ($\Delta F_{anharm}(A \rightarrow TS1) \sim 99$ kJ/mol at 300 K). The reason for this large difference is that the loss of entropy on going from a loosely bound physisorbed propane to a strongly bound Zn-propyl complex (TS1 is a very late transition state close to the intermediate B – chemisorbed propyl and a Brønsted site) is strongly underestimated within hTST. For the inverse reaction (B → TS1) and for the activation of the intermediate to heterolytic dehydrogenation (B → TS2) hTST and thermodynamic integrations yield similar free energies and entropies of activations at $T = 300$ K.

The calculated temperature-dependent reaction rates have been fitted to an Arrhenius equation to derive temperature-independent effective activation energies and prefactors (this is equivalent to the procedure conventionally used to derive activation energies for reaction rates measured at different temperatures). The effective activation energies for the heterolytic H-dissociation (A → TS1) and the corresponding reverse reaction calculated using hTST are lower by a factor of about two than if anharmonicity is correctly taken into account, because the harmonic approach strongly underestimates the loss of entropy upon activation.

In summary, our study leads to important conclusions regarding both the computational methodology and the nature of the active sites in Zn-exchanged mordenite: (i) A location of the Zn^{2+} cation in the center of a six-membered ring at the side wall of the main channel of mordenite is not only an energetically favorable configuration, it forms also a Lewis site of sufficient strength to induce H-dissociation from physisorbed propane. The presence of framework oxygen atoms in the same ring not connected to the Zn^{2+} cation favors the formation of a Brønsted site at a distance from the propyl grafted to the cation which is small enough to facilitate heterolytic H_2 elimination. (ii) Only periodic calculations allow to account for the flexibility of the zeolitic network which is seriously limited even in large clusters. This leads to an overestimation of activation energies in processes where the binding of the reactant is stronger in the transition than in the initial state. (iii) For such reactions, the loss of entropy upon activation may be seriously underestimated by harmonic transition state theory, because soft degrees of freedom such as hindered rotations and translations are not well described in an anharmonic approximation. (iv) Dispersion corrections are important for stabilizing the adsorption of the alkane at the Lewis site. Without dispersion interactions, desorption is favored over H-dissociation.

The present calculations have been performed using a semilocal exchange-correlation functional. It has been argued that hybrid functionals mixing exact (i.e. Hartree-Fock) and density-functional exchange yield more realistic adsorption and activation energies. However, so far calculations based on hybrid functional have been performed almost exclusively for small, eventually embedded clusters. Calculations based on periodic models will be required to further explore the influence of the choice of the functional

Acknowledgment

This work has been supported by the VASP project.

References

[1] T. Mole, J.R. Anderson, G. Creer, Appl. Catal. 17 (1985) 141–154.
[2] L.A.M.M. Barbosa, R.A. van Santen, J. Phys. Chem. C 111 (2007) 8337–8348.
[3] J.A. Biscardi, E. Iglesia, Catal. Today 31 (1996) 207–231.
[4] J.A. Biscardi, G.D. Meitzner, E. Iglesia, J. Catal. 179 (1998) 192–202.
[5] J.A. Biscardi, E. Iglesia, J. Catal. 182 (1999) 117–128.
[6] J.A. Biscardi, E. Iglesia, Phys. Chem. Chem. Phys. 1 (1999) 5753–5759.
[7] V.B. Kazansky, I.R. Subbotina, N. Rane, R.A. van Santen, E.J.M. Hensen, Phys. Chem. Chem. Phys. 7 (2005) 3008–3092.
[8] P.L. De Cola, R. Glaser, J. Weitkamp, Appl. Catal. A: Gen. 306 (2006) 85–97.
[9] S.Y. Yu, J.A. Biscardi, E. Iglesia, J. Phys. Chem. B 106 (2002) 9642–9648.
[10] Y. Sun, T.C. Brown, Int. J. Chem. Kinet. 34 (2002) 467–480.
[11] J. Penzien, A. Abraham, J.A. van Bokhoven, A. Jentys, T.E. Muller, C. Sievers, J.A. Lercher, J. Phys. Chem. B 108 (2004) 4116–4126.
[12] V.B. Kazansky, V. Yu. Borovkov, A.I. Serykh, R.A. van Santen, B.G. Anderson, Catal. Lett. 66 (2000) 39–47.
[13] V.B. Kazansky, E.A. Pidko, J. Phys. Chem. B 109 (2005) 2103–2108.
[14] M.V. Frash, R.A. van Santen, Phys. Chem. Chem. Phys. 2 (2000) 1085–1089.
[15] A.L. Yakovlev, A.A. Shubin, G.M. Zhidomirov, R.A. van Santen, Catal. Lett. 70 (2000) 175–181.
[16] G.M. Zhidomirov, A.A. Shubin, V.B. Kazansky, R.A. van Santen, Theor. Chem. Acc. 114 (2005) 90–96.
[17] V.B. Kazansky, A.I. Serykh, E.A. Pidko, J. Catal. 225 (2004) 369–373.

[18] V.B. Kazansky, V. Yu. Borovkov, A.I. Serykh, R.A. van Santen, B.G. Anderson, Catal. Lett. 66 (2000) 39–47.
[19] V.B. Kazansky, A.I. Serykh, R.A. van Santen, B.G. Anderson, Catal. Lett. 74 (2001) 55–59.
[20] V.B. Kazansky, A.I. Serykh, B.G. Anderson, R.A. van Santen, Catal. Lett. 88 (2003) 211–217.
[21] E.A. Pidko, R.A. van Santen, J. Phys. Chem. C 111 (2007) 2643–2655.
[22] H.A. Aleksandrov, G.N. Vayssilov, Catal. Today 152 (2010) 78–87.
[23] G. Kresse, J. Hafner, Phys. Rev. B 48 (1993) 13115–13118.
[24] G. Kresse, J. Hafner, Phys. Rev. B 49 (1994) 14251–14269.
[25] G. Kresse, J. Furthmüller, J. Comp. Mater. Sci. 6 (1996) 15–50.
[26] G. Kresse, J. Furthmüller, Phys. Rev. B 54 (1996) 11169–11186.
[27] J.P. Perdew, A. Chevary, S.H. Vosko, K.A. Jackson, M.R. Pedersen, D.J. Singh, C. Fiolhais, Phys. Rev. B 46 (1992) 6671–6687.
[28] J.P. Perdew, Y. Wang, Phys. Rev.B 45 (1992) 13244–13249.
[29] P.E. Blöchl, Phys. Rev. B 50 (1994) 17953–17979.
[30] G. Kresse, D. Joubert, Phys. Rev. B 59 (1999) 1758–1775.
[31] A. Heyden, B. Peters, A.T. Bell, F.J. Keil, J. Phys. Chem. B 109 (2005) 1857–1873.
[32] S. Grimme, J. Comput. Chem. 27 (2006) 1787–1799.
[33] J.G. Kirkwood, J. Chem. Phys. 3 (1935) 300–313.
[34] J.P. Ryckaert, G. Ciccotti, H.J.C. Bredesen, J. Comput. Phys. 23 (1977) 327–341.
[35] E.A. Carter, G. Ciccotti, J.T. Hynes, R. Kapral, Chem. Phys. Lett. 156 (1989) 472–477.
[36] T. Bučko, L. Benco, J. Hafner, J.G. Ángyán, J. Catal. 250 (2007) 171–183.
[37] M.P. Allen, D.J. Tildesley, Computer Simulations of Liquids, Oxford Science Publications, Clarendon, Oxford, UK, 1987.
[38] H.C. Anderson, J. Chem. Phys. 72 (1980) 2384–2393.
[39] L. Benco, T. Bucko, J. Hafner, J. Phys. Chem. C 113 (2009) 18807–18816.
[40] L. Benco, T. Bucko, J. Hafner, H. Toulhoat, J. Phys. Chem. B 109 (2005) 20361–20369.
[41] T. Demuth, J. Hafner, L. Benco, H. Toulhoat, J. Phys. Chem. B 104 (2000) 4593–4607.
[42] T. Takaishi, M. Kato, K. Itabashi, Zeolites 15 (1995) 21–32.
[43] W. Löwenstein, Am. Miner. 39 (1954) 92–96.
[44] M. Kato, K. Itabashi, A. Matsumoto, K. Tsutsumi, J. Phys. Chem. B 107 (2003) 1788–1797.
[45] J.D. Cox, G. Pichler, Thermochemistry of Organic and Organometallic Compounds, Academic Press, New York, 1970.
[46] H. Eyring, J. Chem. Phys. 3 (1935) 107–115.
[47] M.H. Evans, M. Polanyi, Trans. Faraday. Soc. 31 (1935) 875–893.
[48] T.J. Frankcombe, G.J. Kroes, Phys. Rev. B 73 (2006). 174301/1–9.
[49] C. Wolverton, V. Ozolins, Phys. Rev. B 75 (2007). 064101/1–15.